Photophysics and Relaxation Dynamics of Ru(4,4′Dicarboxy-2,2′-bipyridine)$_2$cis(NCS)$_2$ in Solution

M. R. Waterland and D. F. Kelley*

Department of Chemistry, Kansas State University, Manhattan, Kansas 66506-3701

Received: November 8, 2000; In Final Form: February 14, 2001

The relaxation and interligand electron-transfer dynamics of Ru(4,4′dicarboxy-2,2′-bipyridine)$_2$cis(NCS)$_2$, the N3-dye, have been studied using femtosecond polarized transient absorption spectroscopy. These studies have been performed in room temperature acetonitrile, methanol, and ethanol solutions. The results indicate that the dynamics are strongly dependent on the solvent and the excitation wavelength; results following 520 and 650 nm excitation are herein reported. These results may be semiquantitatively understood in terms of a model in which the MLCT π^* electron is intrinsically localized on a single bipyridine ligand. In this model, the intersection of the MLCT states associated with each of the bipyridine ligands results in an avoided crossing on the MLCT surface, producing upper and lower MLCT states. 520 nm light primarily populates the upper surface, whereas 650 nm light primarily populates the lower surface. The rate of upper to lower surface relaxation is strongly solvent dependent, varying from about 24 ps in acetonitrile to about 1.1 ns in methanol. There is a large barrier to interligand electron transfer on the lower surface and this process occurs on the 1.5 ns time scale. The results are fit with an interligand electronic coupling of about 200 cm^{-1} and a barrier height of 1050 cm^{-1}.

Introduction

There has recently been great interest in dye sensitized electron injection photovoltaic cells. These cells have achieved high efficiencies and hold considerable promise as a commercially viable technology.[1−3] Charge separation in these cells occurs as a result of visible light photoexcitation of an inorganic dye followed by injection of an electron into a nanoporous TiO_2 electrode. The dye that is typically used is Ru(4,4′dicarboxy-2,2′-bipyridine)$_2$cis(NCS)$_2$, the so-called "N3 dye". N3-dye strongly adsorbs onto the TiO_2 surface and is surrounded by a polar solvent containing an electrolyte.[4,5] Following electron injection, the oxidized N3-dye is reduced to its neutral form by I_3^- in solution. The kinetics of these processes, especially electron injection into TiO_2 and other semiconductors, have been extensively studied.[6−14] Much of the electron injection occurs rapidly, in less than 100 fs. In addition, slower electron injection components have also been reported.

Despite the intense interest in the N3/TiO_2 electron injection dynamics, very little is known about the photophysics and relaxation dynamics of N3-dye in polar solutions. Many important aspects of these photophysics simply have not been explored. The excited state of N3-dye is known to be metal-to-ligand charge transfer (MLCT) in nature, involving charge transfer from the ruthenium d-orbitals to the bipyridine π^* orbitals. One interesting aspect of the N3-dye photophysics involves the nature of this excited MLCT state; specifically, whether the excited electron is localized on a single bipyridine ligand or delocalized over both. If the π^* electron is localized on a single bipyridine, then the next obvious questions are to determine the overall dynamics of interligand electron transfer (ILET) in solution, and what role ILET plays in the overall electron injection dynamics of absorbed N3-dye. These questions have not been previously addressed in the literature, and the dynamics of ILET in solution are addressed here.

Although it is unknown whether the MLCT π^* electron is localized or delocalized in N3-dye, one's first guess might be that N3-dye is analogous to Ru(bpy)$_3^{2+}$, in which there is a good consensus that the π^* electron is intrinsically localized. This conclusion results from several different types of studies, including analysis of the excited-state resonance Raman spectrum, the solvent dependent absorption spectrum, Stark effect spectroscopy, and dynamical studies of interligand electron transfer.[15−28] However, it is possible that bipyridine interaction with the metal d (nominally, t_{2g}) orbitals along with t_{2g} back-bonding to thiocyanate ligands could significantly increase the coupling between the bipyridines and that the π^* electron could be delocalized in the N3-dye case. Without direct experimental evidence, it is impossible to say whether the π^* electron in the N3-dye MLCT state is localized or delocalized. Furthermore, assuming that the π^* electron is localized, there is at present no data which address the question of the ILET rates. The dynamics of ILET are not trivially easy to follow with spectroscopic measurements. Because ILET simply interchanges the environments of the two structurally equivalent bipyridine and thiocyanate ligands, it results in no change in the emission or transient absorption spectra. The ILET dynamics can, however, be elucidated using time-resolved absorption polarization spectroscopy. Linearly polarized light accomplishes two types of selective excitation. First, polarized light selectively excites those N3-dye molecules having an MLCT oscillator most closely aligned with the electric vector of the light, and second, assuming that the MLCT state is localized on a single bipyridine upon photon absorption, photoexcitation selectively excites the particular ruthenium-bipyridine moiety most closely aligned with the electric vector of the light. The second type of photoselection is lost upon ILET. Thus, the polarization kinetics of the any of the features in the transient absorption spectrum which are

* To whom correspondence should be addressed: dfkelley@ksu.edu.

10.1021/jp004111w CCC: $20.00
Published on Web 03/31/2001

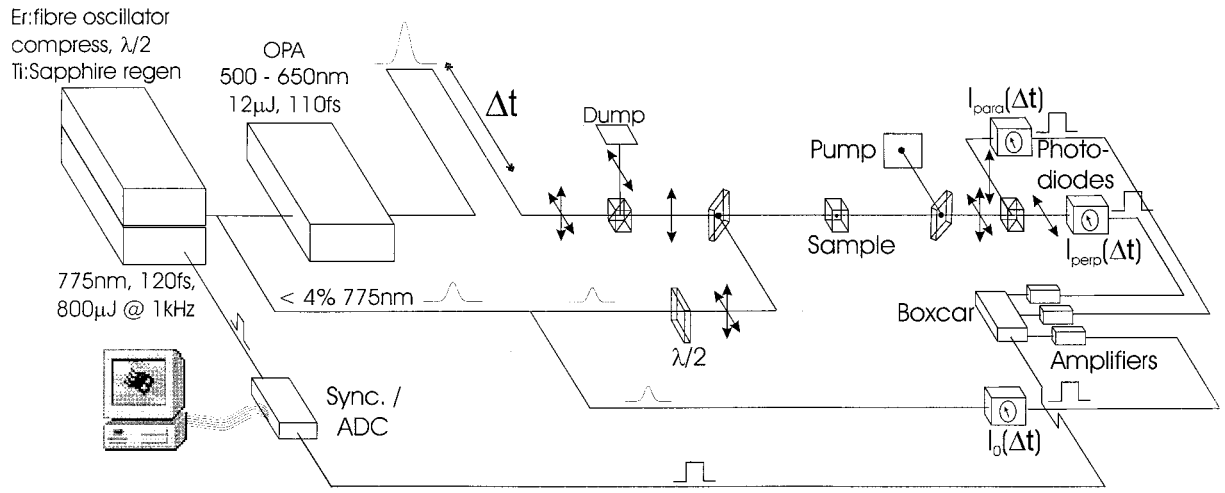

Figure 1. Experimental apparatus used to obtain the results presented here.

sensitive to the presence of the π^* electron may be used to elucidate the ILET dynamics.

In this paper, we report the results of excitation wavelength-dependent time-resolved absorption polarization studies on N3-dye in room-temperature polar solvents. These results show that the MLCT state π^* electron is intrinsically localized on a single bipyridine ligand, that is, localization occurs upon photoexcitation. The results also show that the barrier to ILET is slightly larger than in the $Ru(bpy)_3^{2+}$ case, and that ILET is comparatively slow. In addition, these studies elucidate the dynamics of a higher lying delocalized MLCT state that is formed by the avoided crossing of the localized MLCT states.

Experimental Section

The experimental apparatus used in these studies is shown schematically in Figure 1. The femtosecond light source is based on a Clark-MXR 2001. This produces 775 nm, 130 fs, 800μJ pulses at a repetition rate of 1 kHz. About 4% of the pulse intensity is split off, attenuated, and used for the sample probe. The remainder is used to pump an OPA (Clark-MXR, vis-OPA). The output of the OPA is 10−15 μJ femtosecond pulses, tunable throughout the visible region of the spectrum. This tunable output is used for sample excitation; specifically, results following 520 and 650 nm excitation are presented here. The pump beam is reflected through a corner cube on a delay stage to control the relative arrival time of the pump versus the probe at the sample. This is followed by a Glan−Taylor polarizer, to ensure that the excitation pulse is completely vertically polarized. The pump beam is typically focused to a spot size of 0.5−1.0 mm at the sample. The power density can be varied by changing the position of the sample with respect to the focal point of the pump beam. In the results presented here, variation of the power density by a factor of about 10 has no detectable effect on the observed kinetics.

The low intensity, 775 nm probe beam is attenuated and then split into reference and sample probe components. The sample probe component is then passed through a half wave plate, which is adjusted to obtain equal amounts of vertically and horizontally polarized light. The intensity of the probe pulses is less than 1 μJ at the sample. After the sample, the probe beam is split into horizontal and vertical polarization components. These beams and the I_0 beam are imaged onto UDT Sensors PIN 10D photodiodes, biased at −15 V. The photodiode outputs are amplified and input into an SRS gated integrator. The gated integrator output is measured using a National Instruments 16 bit A/D converter in the data acquisition computer. The A/D converter and gated integrator triggering and reset are synchronized with the CPA 2001 Q-switch and controlled by home-built timing electronics. Data acquisition and movement of the delay stage is controlled by LabView software running on a Pentium II computer.

N3-dye was obtained from Dr. S. Ferrere at NREL and used without further purification. Samples were held in 1 cm path length sealed cells and rapidly stirred with a magnetic stir bar. Sample concentrations were adjusted so the absorbance at the pump wavelength (520 or 650 nm) was about 0.3 to 0.5. Over the course of the experiments, there was no detectable change in the sample absorption spectrum. Acetonitrile was HPLC grade and was purified by distillation over P_2O_5, in a nitrogen atmosphere. Methanol and ethanol were purified by distillation over iodine activated magnesium, in a nitrogen atmosphere. In all cases, samples were filtered with 0.22 μm pore diameter filters and degassed prior to use. N3-dye has labile thiocyanate ligands which are easily hydrolyzed, and we have found that the above purifications are necessary to avoid hydrolysis of the dye.

Results and Discussion

1. N3-Dye Polarization Spectroscopy. The absorption spectrum of N3-dye in methanol is shown in Figure 2. Similar spectra have been previously reported along with emission spectra and results showing that the excited-state lifetime is quite long, >10 ns.[4] The 520 to 650 nm region corresponds to excitation of the lowest MLCT state. This state is best described as having promoted an electron from a ruthenium orbital to a bipyridine π^* orbital. In the N3-dye case, the ruthenium orbital also has considerable thiocyanate character.[29] Previous transient absorption studies have shown that the MLCT excited state exhibits a broad absorption in the red and near-IR regions of the spectrum, peaking at about 730 nm. This transient absorption has been analyzed and discussed by several different groups.[9−11,30] It is clear that this feature may be assigned to a thiocyanate to ruthenium ligand-to-metal charge-transfer (LMCT) transition. For the present discussion, we will assume that the MLCT state π^* electron is localized on a single bipyridine and return to the validity of this assumption later (section 5). With this assumption, we note that the thiocyanates are not equivalent in the MLCT excited N3-dye molecule. Thus, the observed transient LMCT band is a combination of absorptions due to each of the thiocyanates.

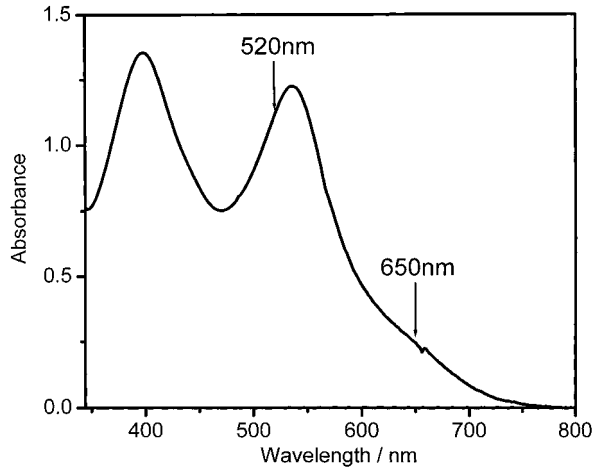

Figure 2. Absorption spectrum of N3-dye in methanol. The excitation wavelengths used in the present study (520 and 650 nm) are also indicated.

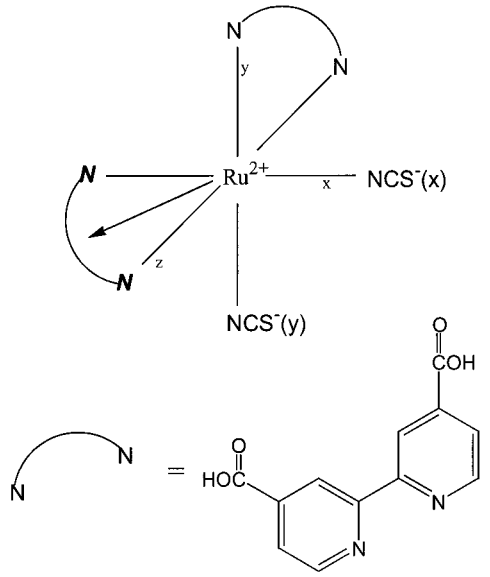

Figure 3. Structure of the N3-dye molecule. The photoselected "reactant" ligand is in the $x-z$ plane and is indicated in bold italics. The dipole vector for this MLCT transition is also shown.

The polarization spectroscopy of N3-dye, specifically the LMCT transitions, is analyzed by considering the ruthenium geometry to be pseudo-octahedral and the MLCT state to be localized on a single bipyridine ligand. The angles involved for MLCT excitation and the thiocyanate to ruthenium LMCT transitions can be derived from the N3-dye diagram shown in Figure 3. The MLCT transition is polarized along the vector which goes through the metal and bisects the photoselected bipyridine. This vector is indicated in Figure 3. Similarly, the LMCT transitions are polarized along the vectors going through the thiocyanates, to the ruthenium. Pump/probe angles of 90° and 135° are obtained for the thiocyanates that are syn (y-axis) and anti (x-axis) with respect to the photoselected bipyridine ligand, respectively. The anisotropy of a transient absorption following excitation with linearly polarized light is given by[31,32]

$$r(t) = (A_{par} - A_{perp})/(A_{par} + 2A_{perp}) = (^2/_5)\, P_2(\cos\theta)\exp(-t/\tau_{rot}) \quad (1)$$

where A_{par} and A_{perp} are the absorption intensities having polarizations parallel and perpendicular to the polarization of the pump pulse, $P_2(\cos\theta)$ is the second Legendre polynomial, $P_2(\cos\theta) = {}^1/_2(3\cos^2\theta - 1)$, θ is the angle between the pump and the probe transitions and τ_{rot} is the rotational diffusion time. Prior to ILET or rotational diffusion, anisotropies of -0.20 and $+0.10$ are calculated for the syn and anti thiocyanates, respectively. Following MLCT excitation, the sample is probed at 775 nm. Because absorption from both LMCT transitions are expected to contribute to the 775 nm absorption, the resulting net anisotropy will be between these two limiting values. ILET exchanges the positions of the thiocyanates relative to the π^* electron, and thus their anisotropies. The resulting net 775 nm absorption anisotropy following ILET is the average of these values, -0.05. The same result is obtained following relaxation to a delocalized state. The conclusions of this discussion are fairly simple. The anisotropy at 775 nm may start out at any value between 0.1 and -0.2, depending on the relative contributions of the two thiocyanates to the total absorption. Following ILET, the anisotropy goes to -0.05 in the absence of rotational diffusion. Rotational diffusion results in complete depolarization of the transient absorption and the anisotropy goes to zero on the rotational diffusion time scale.

The simple model depicted in Figure 3 allows us to consider the effect of solvent relaxation on the intensity and polarization of the 775 nm absorption. The spectral maxima and, hence, 775 nm absorption intensities of each of the LMCT absorptions are expected to vary with the dielectric environment of the N3-dye molecule. The relaxed solvent produces an electric field opposing that of the MLCT dipole. This field has a component along the vector of the anti thiocyanate LMCT transition, that is, the anti LMCT and MLCT vectors have a nonzero dot product. The solvent interaction with the MLCT dipole therefore reduces the energy of that transition and solvation produces a time dependent absorption red shift, toward the 775 nm probe wavelength. Thus, the intensity of the LMCT absorption probed at 775 nm is expected to increase with the dielectric relaxation of the polar solvent. The above considerations suggest that the 775 nm absorption kinetics will be sensitive to the extent of solvent relaxation. This spectral shift is larger for the anti than it is for the syn ligand. Because the absorptions associated with the anti and syn have different anisotropies, the observed absorption anisotropy will also change as solvent relaxation occurs.

2. Model for Interligand Electron Transfer. The proposed model for interligand electron transfer takes the MLCT state to be localized on a single bipyridine and thus corresponds to a large dipole directed along a vector from the ruthenium to the center of one of the bipyridine ligands. In this proposed model, ILET results in this vector changing direction by 120°. Any polar solvent interacts with this electric dipole, and ILET is therefore strongly coupled to the solvent dynamics. A simplified (two-dimensional) diagram indicating the interrelationship between solvent relaxation dynamics and ILET is shown schematically in Figure 4. This model ignores complications associated with the singlet and triplet MLCT states. Intersystem crossing of the nascent, localized singlet state occurs rapidly (less than a few picoseconds) and has the effect of releasing some of the excitation energy into the vibrational degrees of freedom. If the MLCT state is localized on a single bipyridine ligand, then intersystem will do nothing to change the spatial extent of the localized electron or the solvent polarization in this reduced symmetry system, that is, the spin−orbit operator does not connect widely separated spatial regions. Intersystem crossing will simply be a vertical relaxation between higher lying singlet surfaces (not shown in Figure 4) and the triplet surfaces

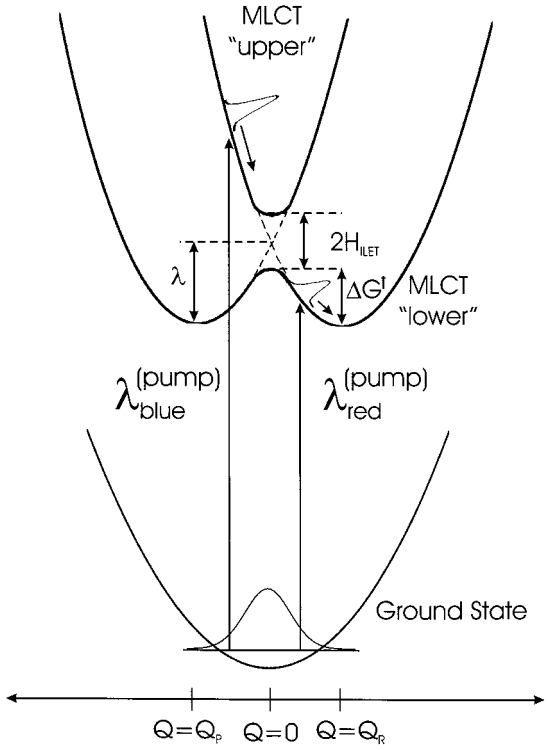

Figure 4. Two-dimensional representation of the potential surfaces used to analyze the time-resolved results. The collective solvent polarization coordinate, Q, is the abscissa. Equilibrium polarizations for the ground state, reactant and product MLCT states are indicated as $Q = 0$, Q_R, and Q_P, respectively. The ground to localized MLCT state solvent reorganization energy is indicated as λ. The ILET activation energy and the electronic coupling between the ligands are indicated as $\Delta G^{\ddagger}$ and H_{ILET}, respectively.

in Figure 4. This does not affect the slower dynamics depicted in Figure 4 and will not be considered further.

According to this model, the solvent is in equilibrium with the ground state charge distribution prior to photoexcitation. At a finite temperature, this equilibrium corresponds to an inhomogeneous, thermal distribution of solvent polarizations around the minimum energy configuration at $Q = 0$, which is depicted in the bottom well of Figure 4. Excitation of the MLCT state results in a large change in dipole moment. In response to the nascent charge distribution, the solvent relaxes to a thermal distribution in equilibrium with that dipole. The ligand which initially has the π^* electron is referred to as the reactant ligand, whereas the ligand that does not have the π^* electron is referred to as the product ligand, see Figure 4. These MLCT states have equilibrium solvent polarizations of Q_R and Q_P, respectively. It is the initial photoselection by the polarized excitation light that defines which ligand is the reactant and which is the product. The potential energy curves associated with solvation of the reactant and product ligands cross at $Q = 0$. This is the ILET transition state and corresponds to the avoided crossing shown in Figure 4. It is important to note that in the two-dimensional model of Figure 4, photoexcitation places population near the ILET transition state. Although the two-dimensional representation of the potential surfaces depicted in Figure 4 is an approximation, the presence of the avoided crossing is independent of this approximation. There will be some solvent polarizations at which the two localized MLCT states have the same energy. The lowest energy solvent polarization at which this occurs is the ILET transition state and an avoided crossing occurs at that point. Figure 4 an easy way to visualize this situation.

Figure 4 shows that the excitation wavelength plays a crucial role in determining the relaxation and ILET dynamics. It is important to note that prior to photoexcitation, there is an inhomogeneous, thermal distribution of Q values, centered at $Q = 0$. Variation of the excitation energy along the Q coordinate results in some of the inhomogeneous width of the absorption spectrum. The value of Q within this inhomogeneous distribution, which is selected by photoexcitation, depends on the wavelength of the excitation light. Excitation on the red edge of the absorption spectrum selects population well away from $Q = 0$ and places it on the reactant surface, below the avoided crossing (see Figure 4). Fairly simple dynamics result from red edge excitation; solvent relaxation is followed by ILET. If the splitting between upper and lower surfaces ($2H_{ILET}$) is sufficiently large that ILET is an adiabatic electron transfer, then the upper surface depicted in Figure 4 is not involved in any of the dynamics. Blue excitation selectively excites population at negative Q values in Figure 4 and places it above the avoided crossing, on the upper surface. This results in more complicated dynamics. Solvent relaxation moves the MLCT population toward the avoided crossing. This population may either go through this avoided crossing on the reactant surface or may get caught on the upper surface at $Q = 0$. The probability of going through the avoided crossing on the zero'th order (reactant) surface may be calculated from Landau−Zener theory,[33−35] and is given in terms of the adiabaticity parameter, H_a, see eq 2.

$$P = \exp(-H_a/2) \text{ and } H_a = \pi H^2_{ILET}\tau_{rlx}/\hbar\lambda \qquad (2)$$

where τ_{rlx} is the solvent relaxation time, and λ is the solvent reorganization energy ($= \Delta G^{\ddagger} + H_{ILET}$). If $P \cong 1$ (i.e., H_{ILET} is small) then very little population gets caught on the upper surface and red and blue excitation give very similar dynamics. However, if $P < 1$ (i.e., H_{ILET} is large), then some fraction of the population gets caught at the upper surface minimum and more complicated dynamics are obtained. Because at $Q = 0$ the upper state is a linear combination of the reactant and product states, the population on the upper surface at $Q \cong 0$ is delocalized and exhibits an anisotropy of -0.05. After being caught in this state, the system "forgets" which zero'th order state it started out on and subsequently relaxes to a 50/50 combination of localized reactant and product populations. Going from a delocalized state to a random mixture of localized states results in no change in absorption anisotropy. However, because of the change in solvation, the absorption maxima of the LMCT transitions will shift upon going from the delocalized, upper state minimum to the localized, reactant and product minima on the lower surface. We therefore expect that the 775 nm absorbance will be sensitive to relaxation from the upper to the lower surface.

A rough estimate of the rate of upper to lower state relaxation may also be obtained from Landau−Zener theory. This estimate is rather crude, however, for the following reason. The usual Landau−Zener result is derived assuming the that prior to a curve crossing event, the system is in a region where the zero'th order states are not mixed and is therefore in a well-defined zero'th order state.[35] The reactant and product states are extensively mixed when the energy is less than about H_{ILET} above that at the avoided crossing, and decreases rapidly at higher energies. For the case of a Boltzmann population distribution in the upper well depicted in Figure 4, the Landau−Zener assumption is valid only when $H_{ILET} \ll kT$. The simplest approximation to account for this is that only the systems more than H_{ILET} above the bottom of the upper well can undergo curve

hopping upon going through the interaction region. For a Boltzmann population distribution in the upper well, the upper to lower surface transition rate may be estimated as

$$k = \frac{1}{2}(1/\tau_{rlx}) \exp(-H_{ILET}/kT) \exp(-\pi H^2_{ILET}\tau_{rlx}/2\hbar\lambda) \quad (3)$$

The factor of $^1/_2$ comes from the fact that only $^1/_2$ of the molecules are moving in the correct direction to undergo curve crossing. With this approximation, eq 3 provides an estimate of the rate at which this Landau−Zener mechanism causes population to relax from the $Q \cong 0$ region of the upper surface to a mix of relaxed reactant and product states. In addition to this mechanism, relaxation may also occur by the usual radiationless decay mechanism, involving vibrational levels on the lower surface.

The above spectroscopic considerations may be summarized as follows. Immediately following excitation, the LMCT absorption intensity measured at 775 nm is expected to be comparatively low and can have an anisotropy anywhere between −0.2 and +0.1. Solvent relaxation shifts the LMCT bands and therefore affects both the intensity and the polarization of the 775 nm transient absorption. We expect that on the lower surface, solvent relaxation will increase the absorption intensity. Because the absorption spectrum of the anti thiocyanate has a positive anisotropy and is expected to red shift more than that of the syn thiocyanate, solvent relaxation is also expected to increase the anisotropy. Subsequent ILET will have no effect on the absorption intensity, but in the absence of rotational diffusion, will cause the anisotropy to go to −0.05. On the upper surface, solvent relaxation produces a delocalized state and will take the anisotropy toward a value of −0.05. Relaxation from the upper to the lower surface will not affect the anisotropy but will affect the absorption intensity. Thus, by observing the time dependence of both the intensity and the polarization of the 775 nm absorption, it is possible to uniquely assign the relaxation and ILET dynamics.

3. Dynamics Following Red Edge (650 nm) Excitation. The transient 775 nm absorption intensity for N3-dye in room-temperature methanol following 650 nm excitation is shown in Figure 5. The absorption intensities polarized parallel (A_{par}) and perpendicular (A_{perp}) to the polarization of the excitation pulse are determined separately and the total absorption intensity is taken to be $A_{par} + 2A_{perp}$. This absorption intensity is independent of polarization effects. Figure 5 shows that this absorption exhibits a pulse width limited rise followed by a slower rise, with a time constant of about 5 ps. Analogous results in ethanol also exhibit a slow component with a rise time of about 20 ps. These rise times are close to the average dielectric relaxation times of methanol (5 ps) and ethanol (15 ps), respectively.[36,37] As discussed above, solvent relaxation is expected to produce an increase in the 775 nm absorption intensity. The 5 and 15 ps rising components are therefore assigned to solvent relaxation on the lower MLCT surface and perhaps vibrational relaxation as well. Solvent relaxation is a complicated nonexponential process,[36,37] that will affect the absorption intensity in a way that is strongly observation wavelength dependent. The emphasis of this paper is the electronic and ILET dynamics rather the solvent relaxation dynamics which occur on somewhat longer time scales, and no attempt to further analyze this the 5 and 20 ps rising components will be made. Following this rise, there is a very small amplitude decay (<10% of the total) on the 700 ps time scale. Scans to longer times show that this absorption intensity decreases very slowly, corresponding to the N3-dye excited-state lifetime (>10 ns).

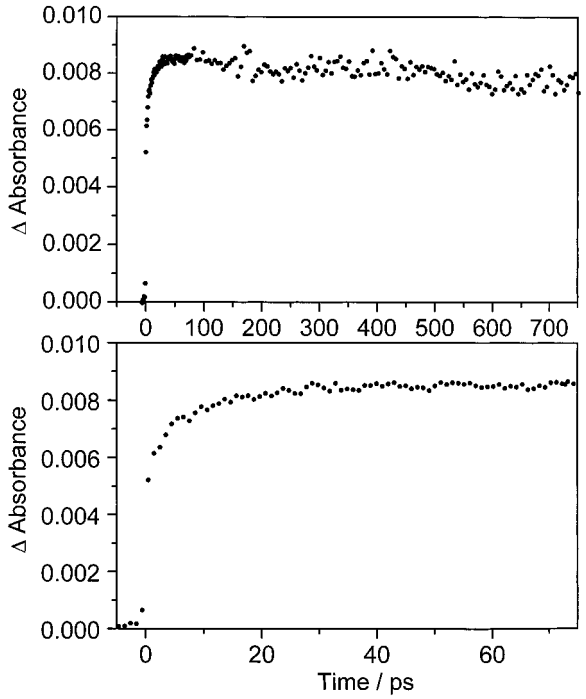

Figure 5. Experimental plots of total absorbance ($A_{PAR} + 2A_{PERP}$) as a function of time for N3-dye in methanol solution, following excitation at 650 nm. The lower panel shows the same data as the upper panel, except on an expanded time scale.

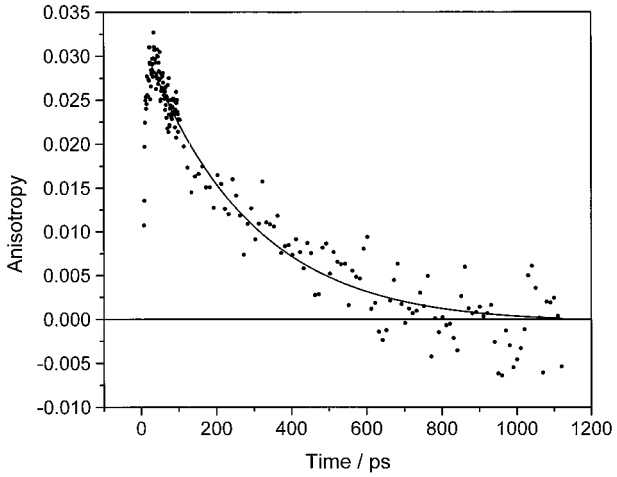

Figure 6. Experimental plots of absorption anisotropy, $(A_{PAR} - A_{PERP})/(A_{PAR} + 2A_{PERP})$, as a function of time for N3-dye in methanol solution, following excitation at 650 nm. Also shown is a curve calculated from eq 4 with an ILET equilibration time, $(2k_{ILET})^{-1}$ of 1.5 ns and a rotational diffusion time of 400 ps.

The anisotropy of the 775 nm absorption (defined by eq 1) is shown in Figure 6. This anisotropy initially increases with a 5 ps time constant, followed by a slower decay. We note that the anisotropy decay proceeds through zero at the end of the 1.2 ns scan and goes slightly negative at later times. These kinetics are assigned to a combination of ILET and rotational diffusion, both occurring on the hundreds of picoseconds to nanoseconds time scale. In the absence of rotational diffusion, the final asymptotic value is predicted to be −0.05 on the basis of photoselection theory, as discussed above. We suggest that the reason that the anisotropy goes only slightly negative is that rotational diffusion results in considerable depolarization of the absorption at longer times. The ILET rate can be easily related to the observed anisotropy decay rate. The anisotropy decay due to ILET is related to the difference in the reactant and

product ligand populations. These populations are related by the following simple set of coupled differential equations.

$$\mathrm{d[reactant]}/\mathrm{d}t = -k_{\mathrm{ILET}}\,([\mathrm{reactant}] - [\mathrm{product}])$$

and

$$\mathrm{d[product]}/\mathrm{d}t = +k_{\mathrm{ILET}}\,([\mathrm{reactant}] - [\mathrm{product}])$$

Solution of these equations gives a population difference that decays at a rate of $2k_{\mathrm{ILET}}$. The anisotropy decays at the same rate. If the asymptotic value of the anisotropy is taken to be -0.05 in the absence of rotational diffusion, then the time dependent anisotropy (following solvent relaxation) is given by

$$r(t) = [r_f + (r_{\mathrm{init}} - r_f)\exp(-2k_{\mathrm{ILET}}\,t)]\exp(-t/\tau_{\mathrm{rot}}) \quad (4)$$

where τ_{rot} is the rotational diffusion time, r_{init} is the initially observed anisotropy, and r_f is the limiting anisotropy, predicted to be -0.05 by photoselection theory. The rotational diffusion time in methanol is taken to be 400 ps (discussed below) and r_{init} and k_{ILET} are taken to be adjustable parameters. We note, however, that theoretically predicted anisotropy of -0.05 may not be realized. We find that variation of r_f in the range of -0.05 to -0.02 has a negligible effect on the calculated curves and only slightly affects the value of k_{ILET} needed to fit the experimental results. The calculated curve shown in Figure 6 corresponds to eq 4 with $r_{\mathrm{init}} = 0.032$ and $2k_{\mathrm{ILET}} = (1.5\ \mathrm{ns})^{-1}$ and taking the limiting anisotropy, $r_f = -0.025$. The results obtained following 520 nm excitation (discussed below) are consistent with this value of a limiting anisotropy.

With the assumption that ILET is an adiabatic electron transfer, the ILET rate permits estimation of the ILET barrier height. This estimate can be made taking into account the solvent relaxation dynamics and the curvature of the electronic surface at the transition state. For a symmetric electron transfer, a simple expression for the rate is derived using continuum theory.[38,39] Specifically

$$k_{\mathrm{ILET}} = \frac{1}{\tau_{\mathrm{rlx}}}\left[\frac{\Delta G^{\ddagger} + H_{\mathrm{ILET}}}{2H_{\mathrm{ILET}}} - 1\right]^{1/2}\frac{\exp(-\Delta G^{\ddagger}/RT)}{2\pi} \quad (5)$$

where $\Delta G^{\ddagger}$ is the solvent induced barrier height. The validity of the adiabatic approximation will be discussed later. Taking $2k_{\mathrm{ILET}} = (1.5\ \mathrm{ns})^{-1}$ and the methanol relaxation time to be 5.0 ps, along with an estimate of H_{ILET} of 200 cm^{-1} (see below), a barrier height of about 1050 cm^{-1} is obtained. A comparable analysis can be applied to the results obtained in acetonitrile, and a comparable ILET rate is obtained. However, ILET in acetonitrile is intermediate between the adiabatic and nonadiabatic limits (discussed below), so this rate is not easily interpreted in terms of the barrier height.

From the above $\Delta G^{\ddagger}$ value (1050 cm^{-1}), and an estimate of H_{ILET} of 200 cm^{-1} an estimate of λ ($= \Delta G^{\ddagger} + H_{\mathrm{ILET}}$, see Figure 4) of 1250 cm^{-1} is obtained. (Note that this is the reorganization energy associated with MLCT excitation depicted in Figure 4, not the reorganization energy of the ILET reaction.) This value makes good sense in terms of the structure of N3-dye and a dielectric continuum model, as can be seen from the following discussion. Each localized MLCT state has a large dipole associated with an electron being transferred to the bipyridine. To calculate λ, the difference between a localized MLCT state dipole and the ILET transition state dipole must be considered. The latter corresponds to a dipole vector $^1/_2$ of the length and bisecting the two localized MLCT state dipole vectors. Consideration of this geometry gives the difference between a localized MLCT dipole vector and the transition state vector. This difference, denoted $\Delta\mu^*$, has a magnitude of $\sqrt{3}/_2$ of the MLCT dipole. Dielectric continuum theory[40] gives the energy associated with creating this dipole as

$$\lambda = (\Delta\mu^{*2}/r_0^{\,3})[(\epsilon_0 - 1)/(2\epsilon_0 + 1) - (\epsilon_\infty - 1)/(2\epsilon_\infty + 1)] \quad (6)$$

where r_0 is the dielectric cavity radius, ϵ_0 and ϵ_∞ are the low and high-frequency dielectric constants, respectively. ϵ_∞ is usually taken to be the square of the refractive index. The quantity in brackets has a numerical value of about 0.31 for both methanol and acetonitrile. A reasonable estimate for r_0 is about 5.5 Å. This is about the distance from the ruthenium to the hydrogens on the bipyridine rings. (The carboxylates extend considerably further, but probably do not exclude much of the solvent from the immediate proximity of the molecule.) With this r_0 value and taking $\lambda = 1250\ \mathrm{cm}^{-1}$, eq 6 gives a $\Delta\mu^*$ value of 11.5 D. This corresponds to a localized MLCT state dipole moment of 11.5 D/($\sqrt{3}/_2$) = 13.3 D, which indicates that the MLCT charge separation is about 2.8 Å. It is of interest to compare the magnitude of the N3-dye MLCT dipole to that in $Ru(bpy)_3^{2+}$. Stark spectroscopy measurements have indicated that the $Ru(bpy)_3^{2+}$ dipole ($\cong$ 7 D) is smaller than the 13.3 D N3-dye dipole calculated here.[23,24] This result may be understood in terms of the molecular geometry and electronic structure calculations. Recent DFT calculations[27] indicate that in N3-dye, the ruthenium t_{2g} orbitals are significantly delocalized onto the thiocyanate ligands, resulting in a slightly longer electron-transfer distance and thus a larger dipole than in the $Ru(bpy)_3^{2+}$ case. We also note that the ILET barrier height in N3-dye is somewhat larger than, but roughly comparable to that obtained for related molecules. Temperature-dependent ESR line width studies have yielded an ILET barrier height for the reduced compound $Ru(bpy)_3^{1+}$, which also has an electron in the bipyridine π^* orbital. In this case, an ILET barrier of 950 cm^{-1} was reported in acetonitrile.[41] The N3-dye barrier height is somewhat larger than the 500 cm^{-1} barrier height obtained for $Os(bipyridine)_3^{2+}$ in an earlier study.[28] These comparisons are also consistent with the MLCT dipole being slightly larger in N3-dye than in the tris-bipyridyl complexes.

4. Dynamics Following Blue (520 nm) Excitation. The total transient 775 nm absorption intensity ($A_{\mathrm{par}} + 2A_{\mathrm{perp}}$) in methanol following 520 nm excitation is shown in Figure 7. Just as in the 650 nm excitation case, the absorption rise has both pulse width limited and slower components. The slower components (5 ps in methanol, 20 ps in ethanol) match the average solvent relaxation time, just as was the case following 650 nm excitation. Unlike 650 nm excitation case, the absorption intensity undergoes a slow partial decay following 520 nm excitation. This component is about $^1/_3$ of the total absorbance and decays with a time constant of about 1.1 ns. An analogous plot for acetonitrile is shown in Figure 8. In the acetonitrile case, the decay is of smaller amplitude (about 15% of the total), and has a much shorter time constant of 24 ps. Also shown in Figure 8 (lower panel) are the kinetics following 650 nm excitation. The comparison between the two excitation wavelengths shows that even though the amplitude of the 24 ps decay is small, it is real, reproducible and not an artifact.

Blue excitation puts much of the population on the upper surface above the avoided crossing (see Figure 4). In the case of methanol, solvent relaxation moves this population to the vicinity of $Q = 0$, where it is temporarily caught on the upper surface. This occurs on the time scale of the average solvent relaxation time, and results in the observed slowly rising

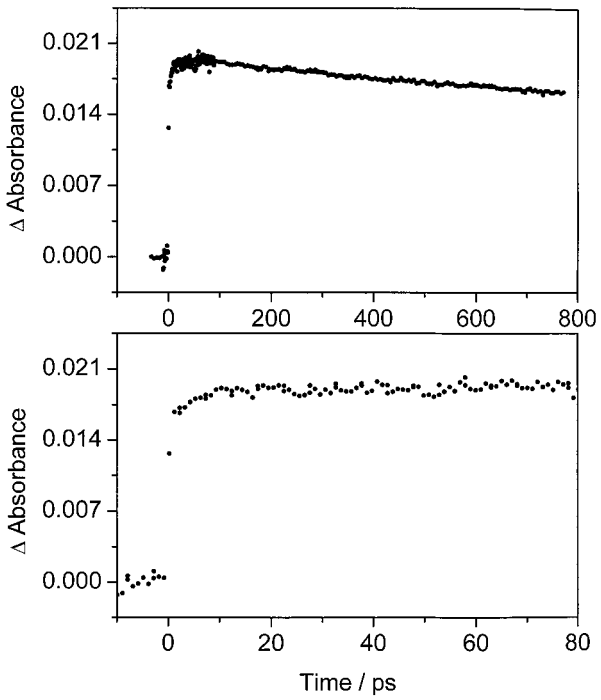

Figure 7. Experimental plots of total absorbance ($A_{PAR} + 2A_{PERP}$) as a function of time for N3-dye in methanol solution, following excitation at 520 nm. The lower panel shows the same data as the upper panel, except on an expanded time scale. Also shown in the upper panel is a calculated curve corresponding to 1100 ps decay having an amplitude which is 34% of the total amplitude. The calculated curve fits the data very well and is therefore barely visible.

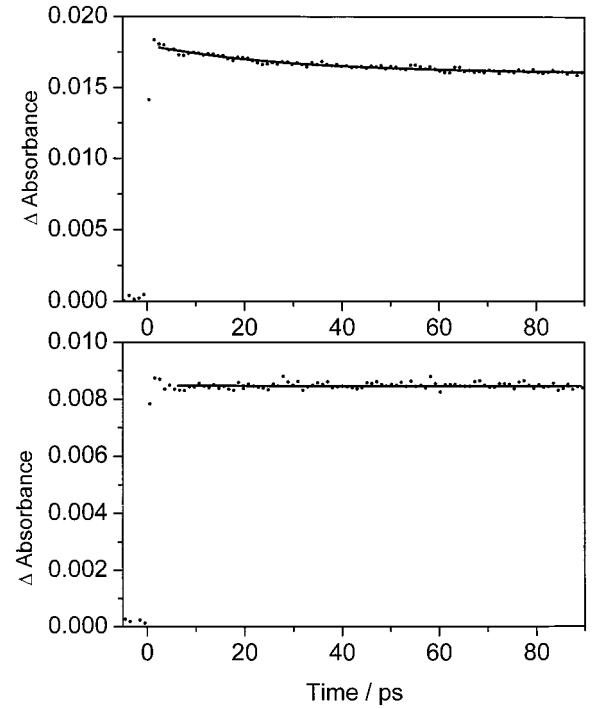

Figure 8. Experimental plots of total absorbance ($A_{PAR} + 2A_{PERP}$) as a function of time for N3-dye in acetonitrile solution, following excitation at 520 nm (upper panel) and 650 nm (lower panel). Also shown is a calculated curve corresponding to 24 ps decay having an amplitude which is 15% of the total amplitude (upper panel) and a horizontal line at an anisotropy of 0.0084 (lower panel).

component (5 ps in methanol, 20 ps in ethanol) of the 775 nm absorption. We infer that subsequent relaxation to the lower surface reduces the 775 nm absorption intensity and is responsible for the 1.1 ns decay observed in the methanol kinetics. The amplitude of this decay in acetonitrile is about $^1/_2$ of that observed in methanol. This result may be understood in terms of a difference in adiabaticity parameter in the two solvents. We suggest that about $^1/_2$ of the population relaxes through the avoided crossing, remaining on the reactant surface. From eq 2, this implies that $0.5 = \exp(-\pi H^2_{ILET}\tau_{rlx}/2\hbar\lambda)$. H_{ILET} may therefore be estimated, knowing the solvent relaxation time. Dielectric relaxation in acetonitrile exhibits a biphasic decay with 90 fs (69%) and 0.63 ps (31%) components.[36] It is appropriate to use the fast relaxation component for this calculation because the avoided crossing is encountered during the initial phase of the relaxation, when the fast component occurs. In this case, a value for H_{ILET} of 180 cm^{-1} is obtained.

Relaxation from the upper to the lower MLCT surfaces may occur by a curve hopping (Landau−Zener) mechanism and/or by a radiationless decay mechanism involving electronic to vibrational energy relaxation. Calculation of the relaxation rate from Landau−Zener theory requires the solvent relaxation time, see eq 3. In this case, the relaxation to the bottom of the upper MLCT state has occurred and the most appropriate value of τ_{rlx} is the average acetonitrile solvent dielectric relaxation time of 0.26 ps. Taking the $H_{ILET} = 180$ cm^{-1} and $\lambda = 1250$ cm^{-1}, eq 3 gives an upper to lower surface relaxation time of 10 ps. This is in reasonably good agreement with the observed time of 24 ps, considering the fairly crude approximations made. Alternatively, H_{ILET} may also be estimated from the observed upper state decay time of 24 ps using eq 3 and an H_{ILET} value of 215 cm^{-1} is obtained. Thus, the kinetics in acetonitrile give two *independent* estimates of H_{ILET}: 180 and 215 cm^{-1}.

It is of interest to try to apply eq 3 to the methanol results. The upper to lower surface relaxation time in methanol is approximately 1.1 ns, which cannot be understood in terms of eq 3 if H_{ILET} is taken to be even close the 180 cm^{-1} to 215 cm^{-1} range. Using the average dielectric relaxation time for methanol (5.0 ps) and an H_{ILET} value of 200 cm^{-1}, eq 3 yields a transition rate of essentially zero. Alternatively, if the transition time is taken to be 1.1 ns, eq 3 yields an H_{ILET} value of 60 cm^{-1}, which is much lower than the value obtained from either of the acetonitrile results. We conclude that the Landau−Zener mechanism is unimportant in the slower relaxing solvent (methanol) and that relaxation occurs by a decay to excited vibrational levels of the lower surface. The relaxation rate is controlled by the Franck−Condon factors coupling the upper state to vibrationally excited levels of the lower state. This is the usual mechanism that controls excited-state lifetimes in inorganic molecules.

The approximately 200 cm^{-1} value of H_{ILET} can be used to calculate the adiabaticity parameter defined in eq 2. Using the appropriate relaxation time for methanol (5 ps), H_A is calculated to be about 95. This means that the ILET reaction is strongly adiabatic in methanol. A similar calculation using a relaxation time appropriate for acetonitrile (0.26 ps) gives $H_A \cong 5$. We conclude that while ILET is close to being adiabatic in acetonitrile, the coupling is small enough that about $^1/_2$ of the nascent upper surface population goes directly through the avoided crossing on the zero'th order surface.

The time dependent 775 nm absorption anisotropies following 520 excitation in methanol and ethanol solvents are shown in Figure 9. In both cases, two kinetic components are observed. There is a fast transient on the 5 ps (methanol) or 20 ps (ethanol) time scale, followed by a slower decay, on the hundreds of picoseconds time scale. The fast transients match the solvent relaxation times and are assigned to relaxation to the bottom of the upper surface depicted in Figure 4. This position on the

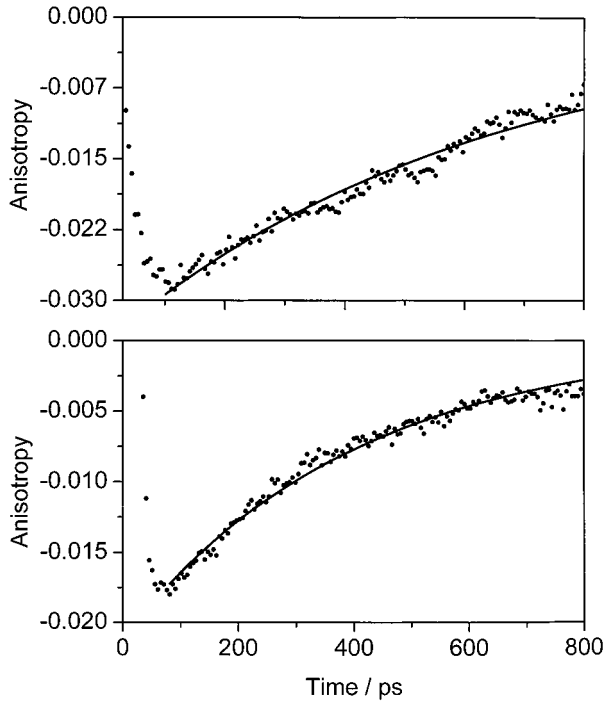

Figure 9. Experimental plots of absorption anisotropy, $(A_{PAR} - A_{PERP})/(A_{PAR} + 2A_{PERP})$, as a function of time for N3-dye in ethanol (upper panel) and methanol (lower panel) solutions, following excitation at 520 nm. Also shown are calculated curves corresponding to rotational diffusion times of 640 and 400 ps in the upper and lower panels, respectively.

potential surface corresponds to a delocalized state, and photoselection theory predicts an anisotropy of -0.05 following this relaxation. Figure 9 shows that the anisotropy reaches a value of -0.02 to -0.03, in semiquantitative agreement with this prediction. As discussed above, subsequent relaxation to a 50/50 mixture of localized reactant and product states is predicted to have no effect on the absorption anisotropies. Thus, rotational diffusion is the only process which can result in loss of this anisotropy. Figure 9 shows that the anisotropy decays to zero with 400 and 630 ps time constants for methanol and ethanol solvents, respectively. In agreement with the assignment to rotational diffusion, the ratio of these decay times is approximately equal to the ratio of solvent viscosities. Furthermore, an approximate hydrodynamic radius may be calculated from these rotational diffusion times using Stokes−Einstein theory. Specifically, if the N3-dye molecule is approximated as a hydrodynamic sphere, the rotational diffusion time is given by $\tau_{rot} = 4\pi r_0^3\eta/3kT$, where r_0 is the hydrodynamic radius and η is the solvent viscosity.[42] The methanol and ethanol results give hydrodynamic radii of 8.75 and 8.1 Å, respectively. This is somewhat larger than was obtained for $Ru(bpy)_3^{2+}$, because of the presence of the carboxylates in N3-dye. It is also somewhat larger than the cavity radius used in the dielectric continuum calculation, above. However, whereas the carboxylates may not exclude much solvent from the immediate proximity of the molecule, they must still move through the solvent for rotation to occur. Inspection of molecular models indicates that the carboxylates extend 8−9 Å from the ruthenium. Calculation of hydrodynamic radii in this range is therefore not surprising.

5. Comparison with $Ru(bpy)_3^{2+}$ and $Os(bpy)_3^{2+}$. It is of interest to compare the results obtained here with those obtained on the closely related and heavily studied molecule, $Ru(bpy)_3^{2+}$. Questions regarding electron localization versus delocalization of the excited MLCT state of $Ru(bpy)_3^{2+}$ have been extensively discussed and debated in the literature. Much of this debate has been regarding whether the MLCT π^* electron is localized upon photoexcitation and, if the π^* electron is initially delocalized, the time scale on which localization occurs. The consensus is now that the π^* electron is intrinsically localized in room-temperature polar solutions. Localization of the π^* electron in $Ru(bpy)_3^{2+}$ or N3-dye may be understood in terms of a straightforward quantum mechanical consideration. This consideration is the comparison of the interaction Hamiltonian, H_{ILET}, with the environmentally induced splitting of the zero'th order, localized MLCT states. This splitting is the energy difference of the bipyridine ligand π^* orbitals. In the gas phase or in a low-temperature crystal where the bipyridines are in equivalent environments, the zero'th order states are degenerate and any finite H_{ILET} couples these states. The resulting eigenstates are linear combinations of the localized zero'th order states and the π^* electron in any of these eigenstates is delocalized. This simple situation is more complicated in a polar solvent environment. In this case, the degeneracy of the zero'th order, localized states is broken by inhomogeneities in the local solvent environment. If the energy differences resulting from environmental inhomogeneities are large compared to H_{ILET} then very little mixing of the zero'th order states occurs and photoexcitation results in a π^* electron which is localized on a single ligand. Alternatively, if the energy differences caused by the local environment are small compared to H_{ILET}, then the states remain mixed and the π^* electron is delocalized. In a room-temperature polar solution, these energies vary with fluctuations in the local solvent. The average energy difference between the localized MLCT states may be calculated using the two-dimensional approximation of Figure 4. With this approximation, the average splitting is $4(\lambda kT/\pi)^{1/2}$, where λ is the solvent reorganization energy, that is, the energy that the solvent releases as it reorients in the electric field of the MLCT dipole. The above expression follows from considering the absolute value of the separation between the reactant and product curves depicted in Figure 4 and integrating this difference over a thermal distribution in the ground-state well. λ may be estimated from a dielectric continuum model using reasonable values for the cavity radius and the MLCT dipole moment. In the case of $Ru(bpy)_3^{2+}$, λ values on the order of 1000 cm^{-1} are obtained. This gives $4(\lambda kT/\pi)^{1/2}$ values of about 1000 cm^{-1} at room temperature. Low-temperature spectroscopic and room-temperature dynamical studies on $Ru(bpy)_3^{2+}$ and closely related molecules indicate that H_{ILET} is at most a few tens of wavenumbers.[25−28,43−49] The comparison of these quantities shows that, in room-temperature solutions, the MLCT π^* electron is localized. $Os(bpy)_3^{2+}$ is very similar to $Ru(bpy)_3^{2+}$. In this case,[28] we estimated that H_{ILET} has a value of about 15 cm^{-1}, and that λ has a value of about 500 cm^{-1}. Just as in the $Ru(bpy)_3^{2+}$ case, H_{ILET} is small compared to $4(\lambda kT/\pi)^{1/2}$ at room temperature ($\cong$1000 cm^{-1}) and the π^* electron is localized. Similarly, $4(\lambda kT/\pi)^{1/2}$ has a value of about 1150 cm^{-1} for N3-dye, which is much larger than H_{ILET}. Of course, if H_{ILET} were large enough to cause delocalization, there would be no double well minimum resulting in "upper" and "lower" surfaces and none of the dynamics shown in Figures 5−8 would occur. The conclusion from these considerations is simple: in these type of compounds, including N3-dye, it is the magnitude of H_{ILET} compared to $4(\lambda kT/\pi)^{1/2}$ that determines whether the π^* electron is localized in a polar solvent. In the N3-dye, $Ru(bpy)_3^{2+}$ and $Os(bpy)_3^{2+}$ cases, H_{ILET} is comparatively small and the π^* electron is intrinsically localized. One recent report has suggested that for $Ru(bpy)_3^{2+}$, the π^* electron is initially delocal-

ized, based on time-resolved absorption anisotropy measurements.[50] However, these results may be interpreted in terms of a localized model which includes the avoided crossings on the MLCT surfaces, similar to the model suggested for $Os(bpy)_3^{2+}$ and the model suggested here for N3-dye.[51]

The roughly 200 cm^{-1} H_{ILET} value obtained here is considerably larger than the values obtained[28] for $Ru(bpy)_3^{2+}$ and $Os(bpy)_3^{2+}$. The larger value in the N3-dye case are due to the presence of thiocyanate ligands. Recent density functional calculations on decarboxylated N3-dye show that the ruthenium d_{xy} orbital along with the π^* orbitals on both thiocyanates (see Figure 3) are common to both localized MLCT states.[29] We infer that interaction of the delocalized ruthenium 4d/thiocyanate π^* orbitals with the "other" bipyridine (i.e., the one on which the π^* electron is not localized) increases the coupling between the localized MLCT states and hence the magnitude of H_{ILET}.

Last, it is of interest to consider the possible relevance of the present results to the electron injection process of N3-dye on TiO_2. N3-dye is known to undergo rapid (subpicosecond) electron injection into nanoporous TiO_2, which provides the basis for the operation of regenerative photovoltaic cells. The present results suggest that if one of the bipyridine ligands is not bound (and therefore not coupled) to the TiO_2 surface, that ILET is far too slow to be important in the overall injection mechanism. However, the evidence suggests that single ligand binding to the surface is not the usual situation.[2,52,53] The conclusion that the delocalized upper state MLCT is quite long-lived compared to the electron injection time suggests that this state may be important in injection dynamics. This type of mechanism may be relevant to the results showing rapid injection from higher excited states.[54,55] Studies of the N3-dye dynamics when it is adsorbed to an inert metal oxide surface may further elucidate the role of this state in the injection process and are currently in progress.

Conclusions

The following conclusions may be drawn from the results presented here:

1. The MLCT state in N3-dye is localized on a single bipyridine ligand, rather than delocalized over both. This localization occurs upon photoexcitation and does not require solvent relaxation. This is analogous to the situation in $Ru(bpy)_3^{2+}$ and $Os(bpy)_3^{2+}$.

2. Interligand electron transfer (ILET) equilibrates population between the two bipyridine ligands slowly, with a time constant of about 1.5 ns. This is because there is a significant solvent polarization induced barrier ($\sim$1050 cm^{-1}) to ILET.

3. The presence of a finite coupling between the localized MLCT states results in an avoided crossing on the MLCT state surface. This produces "upper" and "lower" MLCT states. The upper MLCT state is delocalized in the vicinity of the avoided crossing. The splitting between these surfaces is $2H_{ILET}$ and $H_{ILET} \cong 200$ cm^{-1}.

4. Interligand electron transfer is adiabatic in methanol and in neither the adiabatic nor the nonadiabatic limit in the more rapidly relaxing solvent, acetonitrile. As a result, 520 nm excitation results in almost all of the population getting caught on the upper surface in methanol. In contrast, only about $^1/_2$ of the population gets caught on the upper surface in acetonitrile.

The upper to the lower state relaxation times are strongly solvent dependent. These times are about 1.1 ns in methanol and about 24 ps in acetonitrile. The 24 ps time may be understood in terms of a Landau−Zener surface hopping mechanism. The Landau−Zener mechanism predicts much faster upper to lower surface relaxation in solvents with rapid dielectric relaxation and thus predicts essentially no relaxation in methanol on the nanosecond time scale. In general, both Landau−Zener and radiationless decay mechanisms may contribute to the relaxation rate in both solvents, and the radiationless decay mechanism predicts comparable rates in the two different solvents. We therefore conclude that the relaxation time is dominated by a Landau−Zener mechanism in acetonitrile and a radiationless decay mechanism in methanol.

Acknowledgment. This work was supported by a grant from the U. S. Department of Energy (Grant No. DE-FG03-96ER14717). M.R.W. also thanks the Foundation for Research, Science and Technology of New Zealand for a New Zealand Science and Technology Postdoctoral Fellowship (Contract No. KSU-901). The authors would also like to thank Dr. S. Ferrere for the sample of N3-dye.

References and Notes

(1) Kamat, P. V., Meisel, D., Eds. *Semiconductor Nanoclusters—Physical, Chemical and Catalytic Aspects*; Elsevier: New York, 1997.
(2) Hagfeldt, A.; Gratzel, M. *Acc. Chem. Res.* **2000**, *33*, 269.
(3) Hagfeldt, A.; Gratzel, M. *Chem. Rev.* **1995**, *95*, 49.
(4) Nazeeruddin, M. K.; Kay, A.; Rodicio, I.; Humphry-Baker, R.; Muller, E.; Liska, E. P.; Vlachopoulos, N.; Gratzel, M. *J. Am. Chem. Soc.* **1993**, *115*, 6382.
(5) Oregan, B.; Gratzel, M. *Nature* **1991**, *353*, 737.
(6) Ashbury, J. B.; Ellingson, R. J.; Ghosh, N.; Ferrere, S.; Nozik, A. J.; Lian, T. *J. Phys. Chem. B* **1999**, *103*, 3110.
(7) Ashbury, J. B.; Wang, Y.; Lian, T. *J. Phys. Chem.* **1999**, *103*, 6644.
(8) Ellingson, R. J.; Ashbury, J. B.; Ferrere, S.; Ghosh, H. N.; Sprague, J. R.; Lian, T.; Nozik, A. J. *J. Phys. Chem. B* **1998**, *102*, 6455.
(9) Hannappel, T.; Burfeindt, B.; Storck, W.; Willig, F. *J. Phys. Chem. B* **1997**, *101*, 6799.
(10) Moser, J. E.; Noukakis, D.; Bach, U.; Tachibana, Y.; Klug, D. R.; Durrant, J. R.; Humphry-Baker, R.; Gratzel, M. *J. Phys. Chem. B* **1998**, *102*, 3649.
(11) Hannapple, T.; Zimmermann, C.; Meissner, B.; Burfeind, B.; Stork, W.; Willig, F. *J. Phys. Chem. B* **1998**, *102*, 3651.
(12) Heimer, T. A.; Heilweil, E. J. *J. Phys. Chem. B* **1997**, *101*, 10 990.
(13) Tachibana, Y.; Moser, J. E.; Gratzel, M.; Klug, D. R.; Durrant, J. R. *J. Phys. Chem.* **1996**, *100*, 20 056.
(14) Wang, Y.; Ashbury, J. B.; Lian, T. *J. Phys. Chem. B* **2000**, *104*, 4291.
(15) Bradley, P. G.; Kressn, N.; Hornberger, B. A.; Dallinger, R. F.; Woodruff, W. H. *J. Am. Chem. Soc.* **1981**, *103*, 7441.
(16) Carlin, C. M.; DeArmond, M. K. *Chem. Phys. Lett.* **1982**, *89*, 297.
(17) Carrol, P. J.; Brus, L. E. *J. Am. Chem. Soc.* **1987**, *109*, 7613.
(18) Caspar, J. V.; Westmoreland, T. D.; Allen, G. H.; Bradley, P. G.; Meyer, T. J.; Woodruff, W. H. *J. Am. Chem. Soc.* **1984**, *106*, 3492.
(19) Dallinger, R. F.; Woodruff, W. H. *J. Am. Chem. Soc.* **1979**, *101*, 4391.
(20) Kober, E. M.; Sullivan, B. P.; Meyer, T. J. *Inorg. Chem.* **1984**, *23*, 2098.
(21) McClanahan, S. F.; Dallinger, R. F.; Holler, F. J.; Kincaid, J. R. *J. Am. Chem. Soc.* **1985**, *107*, 4853.
(22) Myrick, M. L.; Blakley, R. L.; DeArmond, M. K.; Arthur, M. L. *J. Am. Chem. Soc.* **1988**, *110*, 1325.
(23) Oh, D. H.; Boxer, S. G. *J. Am. Chem. Soc.* **1989**, *111*, 1130.
(24) Karki, L.; Hupp, J. T. *Inorg. Chem.* **1997**, *36*, 3318.
(25) Cooley, L. F.; Bergquist, P.; Kelley, D. F. *J. Am. Chem. Soc.* **1990**, *112*, 2612.
(26) Malone, R. A.; Kelley, D. F. *J. Chem. Phys.* **1991**, *95*, 8970.
(27) Pogge, J. L.; Kelley, D. F. *Chem. Phys. Lett.* **1995**, *238*, 16.
(28) Cushing, J. P.; Butoi, C.; Kelley, D. F. *J. Phys. Chem. A* **1997**, *101*, 7222.
(29) Rensmo, H.; Lunell, S.; Siegbahn, H. *J. Photochem. Photobio. A* **1998**, *114*, 117.
(30) Das, S.; Kamat, P. V. *J. Phys. Chem. B* **1998**, *102*, 8954.
(31) Tao, T. *Biopolymers* **1969**, *8*, 609.
(32) Albrecht, A. *J. Mol. Spectrosc.* **1961**, *6*, 84.
(33) Landau, L. *Z. Sov. Phys.* **1932**, *1*, 89.
(34) Zener, C. *Proc. R. Soc. Ser. A* **1932**, *137*, 696.
(35) Eyring, H.; Walter, J.; Kimbal, G. *Quantum Chemistry*; Wiley: New York, 1944.

(36) Horng, M. L.; Gardecki, J. A.; Papazyan, A.; Maroncelli, M. *J. Phys. Chem.* **1995**, *99*, 17 311.
(37) Maroncelli, M. *J. Mol. Liquids* **1993**, *57*, 1.
(38) Calef, D. F.; Wolynes, P. G. *J. Phys. Chem.* **1983**, *87*, 3387.
(39) Calef, D. F.; Wolynes, P. G. *J. Chem. Phys.* **1983**, *78*, 470.
(40) Barbara, P. F.; Wlodzimierz, J. *Adv. in Photochem.* **1990**, *15*, 1.
(41) Motten, A. G.; Hanck, K.; DeArmond, M. K. *Chem. Phys. Lett.* **1981**, *79*, 541.
(42) Fleming, G. R. *Chemical Applications of Ultrafast Spectroscopy*; Oxford: New York, 1986.
(43) Riesen, H.; Krausz, E. *Chem. Phys. Lett.* **1993**, *212*, 347.
(44) Riesen, H.; Krausz, E. *J. Chem. Phys.* **1993**, *99*, 7614.
(45) Riesen, H.; Krausz, E. *Chem. Phys. Lett.* **1994**, *217*, 613.
(46) Riesen, H.; Rae, A. D.; Krausz, E. *J. Lumin.* **1994**, *62*, 123.
(47) Riesen, H.; Wallace, L.; Krausz, E. *Chem. Phys. Lett.* **1994**, *228*, 605.
(48) Riesen, H.; Wallace, L.; Krausz, E. *Chem. Phys. Lett.* **1995**, *198*, 269.
(49) Striplin, D. R.; Crosby, G. A. *Chem. Phys. Lett.* **1994**, *221*, 426.
(50) Yeh, A. T.; Shank, C. V.; McCusker, J. K. *Science* **2000**, *289*, 935.
(51) Kelley, D. F., to be published.
(52) Finnie, K. S.; Bartlett, J. R.; Woolfrey, J. L. *Langmuir* **1998**, *14*, 2744.
(53) Patthey, L.; Rensmo, H.; Perrson, P.; Brohwiler, P. A.; Siegbaum, H.; Lunnel, S.; Martensson, N. *J. Chem. Phys.* **1999**, *110*, 5913.
(54) Ferrere, S.; Gregg, B. A. *J. Am. Chem. Soc.* **1998**, *120*, 843.
(55) Moser, J. E.; Gratzel, M. *Chimia* **1998**, *52*, 160.